Progress In Electromagnetics Research B, Vol. 63, 1–15, 2015

Wide-Band Chaotic Noise Signal for Velocity Estimation and Imaging of High-Speed Moving Targets

Qilun Yang[1, 2, *], Yunhua Zhang[1, 3], and Xiang Gu[1, 3]

Abstract—This paper proposes a burst model of chaotic noise signals with randomly stepped carrier frequencies for velocity estimation and high-resolution range imaging of high-speed moving targets. The random stepping of carrier frequencies is controlled by a combination chaotic map (CCM), which is generated by embedding a Logistic map into a Bernoulli map. The baseband noise signal adopts the CCM based frequency-modulation (CCM-FM) signal, which has good randomness and a thumbtack ambiguity function as well. The velocity estimation includes a coarse search and a precise search, where the coarse search is conducted with a fixed step to makes the velocity deviation less than the velocity resolution, while the precise search adopts the Golden Section Search (GSS) algorithm to get an accurate estimation of velocity. What should be emphasized is that the velocity estimation process can be completed with just a burst of subpulses. Then the spectra are coherently synthesized to obtain ultra-wide bandwidth and high-resolution range imaging. Finally, numerical simulations demonstrate a good performance of the proposed signal model and the processing algorithm.

1. INTRODUCTION

Modern radars are facing increasingly complicated electromagnetic environment along with the development of electronic warfare [1, 2], so the electronic counter-countermeasures (ECCM) capability, low probability of detection and interception (LPD/LPI) characteristics are becoming important research and development directions for military radars [3, 4]. Noise radars have attracted more and more attention owing to their random waveforms, efficient spectrum utilization, good ECCM capability and LPD/LPI characteristics [5–7].

High-resolution radar usually needs wideband signal, so correspondingly very high rate of data sampling is required according to the Nyquist sampling theorem. To obtain ultra-wide synthesized bandwidth while keep low instantaneous bandwidth, stepped-frequency signal is proposed [8, 9]. But the size of frequency step restricts the non-ambiguity range interval [10], so it may suffer from ambiguous peaks, known as "grating lobes" [11]. To overcome this drawback, researchers proposed stepped-frequency Chirp signal (SFCS), which consists of narrow-band sub-chirps with linearly increased/decreased carrier frequencies [12–14], but SFCS is susceptible to coherent jamming [15, 16]. After that, Chirp signal is replaced by noise signal, so as to obtain the stepped-frequency noise signal (SFNS) [17], which can further elevate the anti-jamming capability.

However, the hostile jammer can still easily detect the linearly increased/decreased carrier frequencies and make jamming [18, 19]. In order to further increase the LPD/LPI characteristics and ECCM capability, we incorporate randomly stepped carrier frequencies with a baseband noise signal to form a wideband noise signal.

Received 4 March 2015, Accepted 19 May 2015, Scheduled 20 May 2015

* Corresponding author: Qilun Yang (yangqilun110@163.com).

[1] The Key Laboratory of Microwave Remote Sensing, Chinese Academy of Sciences, Beijing 100190, China. [2] University of Chinese Academy of Sciences, Beijing 100049, China. [3] Center for Space Science and Applied Research, Chinese Academy of Sciences, Beijing 100190, China.

In early times, noise sources are mainly thermal noises [20–22], but their generation is hard to control and their performance is hard to predict as well. With the development of chaotic theory, more and more researchers adopt chaotic signals as pseudo-noise signals. Chaotic signal is a kind of pseudo-random signal generated from a deterministic system. Compared with traditional noise signals, chaotic signal is much easier to generate and control, also the cost is lower [23, 24].

Noise radars not only demand random waveforms, but also incoherent waveforms, i.e., each waveform should be incoherent with one another. It has been shown in [25] that using digital devices, e.g., FPGA chip, to real-time generate chaotic noise signals is a good choice. However, the quantization length is usually very low in FPGA [26], which may destroy the chaotic property. Therefore, we proposed the combination chaotic map (CCM), which is insensitive to the quantization and can keep good chaotic property even though the quantization length is low [25, 27]. The stepping of carrier frequencies is controlled randomly by a CCM sequence and the baseband noise signal adopts the CCM based frequency-modulation (CCM-FM) signal [27].

The high-resolution imaging of high-speed moving targets requires that the velocity should be accurately estimated first. Based on the thumbtack ambiguity function of CCM-FM signal, we propose a new search algorithm for velocity estimation, which just needs a burst of subpulses. The algorithm includes a coarse search and a precise search, where the coarse search is conducted with a fixed step to make the velocity deviation be less than the velocity resolution, while the precise search adopts the Golden Section Search (GSS) algorithm to get the accurate velocity estimation. Next, the high-resolution range imaging can be realized by coherent synthesis of subpulses bandwidths [17, 28].

The rest of the paper is organized as follows. Section 2 introduces the signal model; Section 3 presents the high-resolution range imaging algorithm of high-speed moving targets; Section 4 conducts numerical simulations; Finally, Section 5 draws the conclusion.

2. SIGNAL MODEL

2.1. Wide-Band Chaotic Noise Signals with Randomly Stepped Carrier Frequencies

The investigated wide-band chaotic noise signal consists of a burst of subpulses, whose carrier frequencies are stepped randomly rather than linearly, and each subpulse adopts a narrowband chaotic signal as the pseudo-noise signal. Hence, the sampling rate only needs to satisfy the Nyquist sampling rate for narrowband chaotic signal.

Suppose the start carrier frequency is f_0 and frequency step is Δf. Thus the randomly stepped carrier frequency of the nth subpulse is $f_n = f_0 + c_n \Delta f$, where $c_n \in \{0, 1, \ldots, N-1\}$ is the frequency-hopping code and N is the number of subpulses in a burst. Here, the frequency-hopping code is controlled randomly by a CCM sequence. The bandwidth of each subpulse is B, so the synthesized bandwidth is $B_{syn} = (N-1) \cdot \Delta f + B$. In order to avoid grating lobes, the subpulse bandwidth should be equal to or larger than the frequency step [29].

Figure 1 shows the structure of the proposed signal model, which can be mathematically expressed

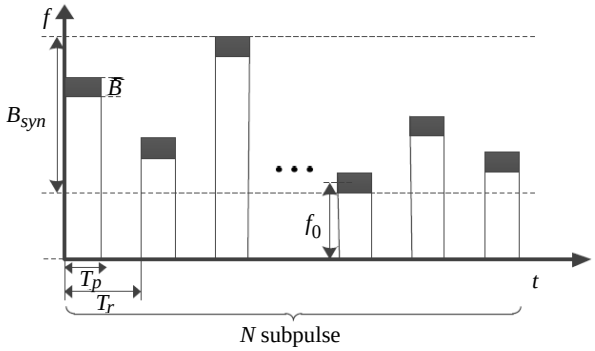

Figure 1. Wide-band chaotic noise signal with randomly stepped carrier frequencies.

as

$$\begin{aligned} s(t) &= g_n\left(\hat{t}\right) \cdot \exp(j2\pi f_n t) \cdot \mathrm{rect}\left(\frac{t - nT_r}{T_p}\right) \\ \hat{t} &= t - t_n, \quad 0 \le \hat{t} \le T_p; \\ t_n &= nT_r, \quad n = 0, 1, \ldots, N-1; \end{aligned} \tag{1}$$

where $g_n(\hat{t})$ is the baseband noise signal of the nth subpulse, which adopts the CCM-FM signal, t_n the instant time of the nth subpulse, T_r the subpulse interval, $\hat{t}$ the fast-time, T_p the time duration (TD) of each subpulse, and rect$(\cdot)$ the rectangle window,

$$\mathrm{rect}(x) = \begin{cases} 1, & 0 \le x \le 1 \\ 0, & \text{otherwise} \end{cases} \tag{2}$$

2.1.1. Combination Chaotic Map

Chaotic maps are sensitive to the control parameters and initial values, i.e., if the control parameter or the initial value have a very tiny change, the generated chaotic sequences will be completely different [30].

General digital devices, e.g., FPGA, usually have limited quantization length. When a chaotic signal is generated in a digital device, the maximum period of a chaotic signal is restricted by the quantization length, and short quantization length may destroy the chaotic property. To keep a good chaotic property even if the quantization length is short, the CCM was proposed [27].

Table 1. One-dimensional chaotic maps for CCM.

Map	Definition	Range of parameter	Range of function
Logistic	$x_{n+1} = u \cdot x_n \cdot (1 - x_n)$	$3.569945 < u \le 4$	$0 < x_n < 1$
Bernoulli	$x_{n+1} = \begin{cases} Bx_n + \frac{1}{2}, & x_n < 0 \\ Bx_n - \frac{1}{2}, & x_n \ge 0 \end{cases}$	$1.4 < B < 2$	$-\frac{1}{2} \le x_n \le \frac{1}{2}$

The CCM is generated by embedding a Logistic map into a Bernoulli map, which are shown in Table 1 [31]. The generation procedure of CCM is: 1) employ the Logistic map to generate the parameters for Bernoulli map; 2) combine the Bernoulli map sequences under different parameters to obtain the CCM sequence. In addition, the formulation of the CCM is as follows,

$$\begin{cases} x_{p+1} = u \cdot x_p \cdot (1 - x_p) & 0 < x_p < 1 \\ B_p = 1.4 + 0.6 \cdot x_p & 0 \le p \le P \\ y_{p,q+1} = g(y_{p,q}) = \begin{cases} B_p y_{p,q} + 0.5, & y_{p,q} < 0 \\ B_p y_{p,q} - 0.5, & y_{p,q} > 0 \end{cases} & 0 \le q \le Q \\ \phi = \{\{y_{0,0}, y_{0,1}, \ldots, y_{0,Q}\}, \{y_{1,0}, y_{1,1}, \ldots, y_{1,Q}\}, \ldots, \{y_{P,0}, y_{P,1}, \ldots, y_{P,Q}\}\} \end{cases} \tag{3}$$

where $\{x_p\}$ is the Logistic map sequence, $\{y_{p,q}\}$ the Bernoulli map sequence under the parameter B_p, and $\{\phi\}$ the generated CCM sequence. In (3), the range of Logistic map sequence is (0, 1), so it needs to be transformed to the interval of (1.4, 2) so as to get the parameters for Bernoulli map.

If the quantization length is K bit, then the maximum period of a general one-dimensional chaotic map will not exceed 2^K. Suppose the period of a Logistic map is 2^{K_1} $(K_1 \le K)$ and that of a Bernoulli map is 2^{K_2} $(K_2 \le K)$, then the maximum period of CCM will be at the magnitude of $\underbrace{2^{K_2} \cdot 2^{K_2} \cdots 2^{K_2}}_{2^{K_1}} = 2^{K_1 \cdot K_2}$ [27], which is much longer than 2^K. Therefore, the CCM is insensitive to the quantization length, i.e., it can keep good chaotic property even though the quantization length is short.

2.1.2. Randomly Stepped Carrier Frequencies

The CCM is adopted to control the stepped carrier frequencies randomly, and the generation of a frequency-hopping code based on CCM is as follows:

1) Generate the CCM sequence, whose range is $\phi_n \in [-\frac{1}{2}, \frac{1}{2}]$.
2) Transform the range of CCM sequence to the range of a frequency-hopping code $c_n \in \{0, 1, \ldots, N-1\}$ by the following transformation:

$$\phi_n^* = \left\lfloor \left(\phi_n + \frac{1}{2}\right) * N \right\rfloor \tag{4}$$

where $\lfloor(\phi_n + \frac{1}{2}) * N\rfloor$ is the largest integer which is equal to or less than $(\phi_n + \frac{1}{2}) * N$.
3) Owing that the adjacent values of ϕ_n^* are of strong iterative relationship, so we extract one from every m values to form a new sequence, i.e.,

$$\hat{\phi}_n = \phi_{n*m}^*, \quad n \in \left[0, \left\lfloor \frac{N}{m} \right\rfloor\right] \tag{5}$$

4) The sequence $\hat{\phi}_n$ may have some equivalent values, so we just extract the different values from start to end to obtain the hopping-frequency code c_n.

Owing the chaotic map is sensitive to the initial value, so we can easily generate different frequency-hopping codes by using different initial values. Next in Section 4, we will conduct simulations to demonstrate this.

2.1.3. Baseband CCM-FM Signal

The CCM sequence is once again utilized to modulate the radar signal frequency so as to obtain the CCM-FM signal, which is used as the baseband noise signal. The discrete formulation of the CCM-FM signal can be expressed as

$$g(n) = A \exp\left\{ j2\pi \sum_{i=0}^{n} \phi_i \right\} \tag{6}$$

The ambiguity function describes the matched-filtering results when the time delay is τ and the Doppler frequency is f_d, and it is a common tool for investigating radar signals [32]. The ideal ambiguity function should be thumbtack, and the definition of the ambiguity function of $g(t)$ [33] is

$$|\chi(\tau, f_d)|^2 = \left| \int_{-\infty}^{\infty} g^*(t) g(t-\tau) \exp(-j2\pi f_d t) dt \right|^2 \tag{7}$$

Let $f_d = 0$, we obtain the range cut of the ambiguity function

$$|\chi(\tau, 0)|^2 = \left| \int_{-\infty}^{\infty} g^*(t) g(t-\tau) dt \right|^2 \tag{8}$$

Obviously, the range cut of the ambiguity function is just the matched-filtering output [34, 35]. Owing to the noise-like property, the range cut is close to a Dirac function. We know that $\tau = \frac{2r}{c}$ and $dr = \frac{c}{2B}$, where r is the range, c is the light speed, dr is the range resolution and B is the signal bandwidth, respectively. Hence, the time delay resolution is

$$d\tau = \frac{2dr}{c} = \frac{2 \cdot \frac{c}{2B}}{c} = \frac{1}{B} \tag{9}$$

Let $\tau = 0$, we have the Doppler cut of the ambiguity function

$$\begin{aligned} |\chi(0, f_d)|^2 &= \left| \int_{-\infty}^{\infty} g^*(t) g(t) \exp(-j2\pi f_d t) dt \right|^2 = \left| \int_{-\infty}^{\infty} |g(t)|^2 \exp(-j2\pi f_d t) dt \right|^2 \\ &= \left| \int_{-T_p/2}^{T_p/2} A^2 \exp(-j2\pi f_d t) dt \right|^2 = \left| A^2 \frac{\sin(\pi f_d T_p)}{\pi f_d T_p} \right|^2 \end{aligned} \tag{10}$$

where T_p is the TD of the CCM-FM signal. We can see that the Doppler cut is a SINC function, and the Doppler resolution df_d is determined by T_p

$$df_d = \frac{1}{T_p} \tag{11}$$

The relation between the velocity v and the Doppler frequency f_d is

$$f_d = \frac{2vf_c}{c} \tag{12}$$

Hence the velocity resolution is

$$dv = df_d \cdot \frac{c}{2f_c} = \frac{c}{2f_c \cdot T_p} \tag{13}$$

It is indicated that the velocity resolution is related to both the TD and the carrier frequency. Moreover, longer TD and higher carrier frequency will lead to better velocity resolution. When the carrier frequency is fixed, the velocity resolution is inversely proportional to the TD. Similarly, when TD is fixed, the velocity resolution is inversely proportional to the carrier frequency.

Let $\tau = 0$ and $f_d = 0$, then the ambiguity function will have the maximum output

$$|\chi(0,0)|^2 = \left|\int_{-\infty}^{\infty} g^*(t)g(t)dt\right|^2 = \left|\int_{-\infty}^{\infty} |g(t)|^2 dt\right|^2 \tag{14}$$

However, when $|\tau| > d\tau$ and $|f_d| > df_d$, $g(t)$ is incoherent with $g(t-\tau)$. So $g^*(t)g(t-\tau)$ is just the noise floor, and its Fourier transformation is also the noise floor. Therefore, the ambiguity function of CCM-FM signal is thumbtack.

2.2. Echo Signal

Suppose that the initial distances between a radar and targets (scattering centers) are R_k ($k = 1, 2, \ldots, K$) and that the targets have the same initial velocity v and same acceleration a. v is positive when the targets move toward the radar, while it is negative when the targets move away from the radar. The same is true for a. The instant ranges of radar targets are

$$R_k\left(t_n, \hat{t}\right) = R_k - v\left(t_n + \hat{t}\right) - \frac{1}{2}a\left(t_n + \hat{t}\right)^2 \tag{15}$$

Therefore, the echo signal is

$$s_r\left(t_n, \hat{t}\right) = \sum_{k=1}^{K} A_k g_n\left[\hat{t} - \frac{2R_k(t_n, \hat{t})}{c}\right] \cdot \exp\left[j2\pi f_n\left(t - \frac{2R_k\left(t_n, \hat{t}\right)}{c}\right]\right. \tag{16}$$

The baseband echo signal is obtained through down-conversion by a radar receiver:

$$\begin{aligned} s_{br}\left(t_n, \hat{t}\right) &= \sum_{k=1}^{K} A_k g_n\left[\left(1 + \frac{2v + 2at_n + a\hat{t}}{c}\right)\hat{t} - \frac{2R_k}{c} + \frac{2vt_n}{c} + \frac{at_n^2}{c}\right] \\ &\quad \cdot \exp\left[-j2\pi f_n\left(\frac{2R_k}{c} - \frac{2v\left(t_n + \hat{t}\right)}{c} - \frac{a\left(t_n + \hat{t}\right)^2}{c}\right)\right] \\ &\approx \sum_{k=1}^{K} \tilde{A}_k g_n\left[\hat{t} - \frac{2R_k}{c} + \frac{2vt_n}{c}\right] \cdot \exp\left(\frac{j4\pi f_n v t_n}{c}\right) \cdot \exp\left(\frac{j4\pi f_n v\hat{t}}{c}\right) \cdot \exp\left[\frac{j2\pi f_n a(t_n + \hat{t})^2}{c}\right] \end{aligned} \tag{17}$$

where $\tilde{A}_k = A_k \exp(\frac{-j4\pi f_n R_k}{c})$, and the time scaling of the echo can be ignored owing to $v \ll c$ and $a \ll c$, i.e., $1 + \frac{2v + 2at_n + a\hat{t}}{c} \approx 1$. We further transform the baseband echo signal from time domain to

frequency domain, i.e.,

$$S_{br}(t_n,f) = \left\{\sum_{k=1}^{K}\tilde{A}_k G_n(f-f_{dn})\cdot\exp\left(\frac{-j4\pi f R_k}{c}\right)\cdot\exp\left[\frac{j4\pi(f+f_n)vt_n}{c}\right]\right\} \otimes\left\{F\left[\exp\left[\frac{j2\pi f_n a\left(t_n+\hat{t}\right)^2}{c}\right]\right]\right\} \tag{18}$$

where $G_n(f)$ is the spectrum of $g_n(\hat{t})$;
$f_{dn}=\frac{2vf_n}{c}$ is the Doppler frequency corresponding to the nth carrier frequency f_n;
$\exp(\frac{-j4\pi f R_k}{c})$ attributes to the initial range induced phase of the kth target;
$\exp(\frac{j4\pi f v t_n}{c})$ accounts for the range migration during the nth subpulse;
$\exp(\frac{j4\pi f_n v t_n}{c})$ is induced by the Doppler effect of the nth subpulse;
$\otimes$ is the convolution operation, F is the Fourier transform and $\exp[\frac{j2\pi f_n a(t_n+\hat{t})^2}{c}]$ is resulted from the acceleration.

3. RANGE IMAGING OF HIGH-SPEED MOVING TARGETS

The high-resolution range imaging algorithm for high-speed moving targets using the investigated signal can be briefly summarized as two steps: 1) subpulse compression and velocity estimation; 2) coherent synthesis of subpulses' bandwidths after motion compensation according to the estimated velocity.

3.1. Subpulse Compression and Velocity Estimation

We just need a burst of subpulses, whose TD is usually very short for velocity estimation of high-speed targets. Hence the velocity variation resulted from acceleration is very small, thus we can ignore the acceleration in signal processing.

The echo of a stationary target is just the time delayed version of the transmitted signal, while the echo of a moving target will be incorporated with the Doppler frequency besides time delay. Suppose the reference velocity and the reference range are v_{ref} and R_{ref}, respectively. Similar to Eq. (18), the baseband reference signal in frequency domain is

$$S_{ref}(t_n,f) = G_n\left(f-f_{dn\_ref}\right)\cdot\exp\left(\frac{-j4\pi f R_{ref}}{c}\right)\cdot\exp\left[\frac{j4\pi(f+f_n)v_{ref}t_n}{c}\right] \tag{19}$$

where f_{dn_ref} is the Doppler frequency corresponding to the reference velocity. Then the subpulse compression by matched-filtering in frequency domain is conducted as

$$\begin{aligned} S(t_n,f) &= S_{br}(t_n,f)\cdot S^*_{ref}(t_n,f) \\ &= \left\{\sum_{k=1}^{K}\tilde{A}_k G_n(f-f_{dn})\cdot G_n^*\left(f-f_{dn\_ref}\right)\cdot\exp\left[\frac{-j4\pi f\Delta R_k}{c}\right]\cdot\exp\left[\frac{j4\pi(f+f_n)\Delta v t_n}{c}\right]\right\} \\ &\quad\otimes\left\{F\left[\exp\left[\frac{j2\pi f_n a(t_n+\hat{t})^2}{c}\right]\right]\right\} \end{aligned} \tag{20}$$

where $\Delta R_k = R_k - R_{ref}$, and $\Delta v = v - v_{ref}$. Moreover, the subpulse compression result in time domain is:

$$\Re_n = F^{-1}\left\{S(t_n,f)\right\} \tag{21}$$

Notice that the ambiguity function of the CCM-FM signal is thumbtack, when the Doppler frequency is larger than the Doppler resolution, i.e., the velocity deviation is larger than the velocity resolution; the ambiguity function output will locate at the sidelobe region. Meanwhile, the mainlobe of the Doppler cut is a SINC function. Therefore, we propose a search algorithm based on the thumbtack ambiguity function, which just need a burst of subpulses to estimate the velocity of a high-speed moving target. The search algorithm includes a coarse search and a precise search, which are presented as follows.

3.1.1. Coarse Search

We know that the velocity cut of the ambiguity function of the CCM-FM signal is a SINC function. Only when the deviation between the reference velocity and the target velocity is less than the velocity resolution, there will be a prominent peak after subpulse compression. In addition, as for the SINC function, when the velocity deviation is $\frac{dv}{2}$, where dv is the velocity resolution, the pulse compression peak just decreases about 3 dB [36]. Therefore, in the coarse search, the reference velocity increases from zero with a fixed step of $\frac{dv}{4}$, by which we can guarantee that the reference velocity will not exceed the target velocity. Meanwhile, owing that we do not know the target direction in advance, so we need to search in two directions, i.e., toward or depart from the radar.

In order to get stable results, we average the matched-filtering results of the N subpulses to obtain $\bar{\Re}$. Then we set the objective function as the peak-average ratio, i.e., the ratio of the peak amplitude $\bar{\Re}_{peak}$ to the average amplitude $\bar{\Re}_{mean}$. The threshold of $\frac{\bar{\Re}_{peak}}{\bar{\Re}_{mean}}$ can be determined based on the peak-sidelobe ratio (PSLR) of the CCM-FM signal, whose unit is decibel. When

$$20 * \log 10 \left(\frac{\bar{\Re}_{peak}}{\bar{\Re}_{mean}} \right) > -PSLR \tag{22}$$

it is thought that the velocity deviation is less than the velocity resolution. When a target moves toward the radar, the velocity after the coarse search will be $v_{coarse} \subset (v - dv, v)$. On the contrary, when target moves apart from the radar, the velocity after the coarse search will be $v_{coarse} \subset (v, v + dv)$.

3.1.2. Precise Search

We know that the mainlobe of SINC function is a convex function, and it has only one peak. Therefore, we can take the simple GSS algorithm to get an accurate estimation for the velocity. The Golden Section Search is to find the extremum (maximum or minimum) by sequentially narrowing the range within which the extremum exists [37–41].

Figure 2 shows the GSS algorithm, whose steps are explained as follows:

Step 1): Set the initial velocities. When the velocity after coarse search is positive, i.e., the target moves toward the radar, the initial value is set as $v_a = v_{coarse}$ and $v_b = v_{coarse} + dv$. Meanwhile, when the velocity after coarse search is negative, i.e., the target moves away from the radar, the initial value is $v_a = v_{coarse} - dv$ and $v_b = v_{coarse}$. Next, we turn to Step 2).

Step 2): Select the two reference velocities as $x_1 = v_b - 0.618 * (v_b - v_a)$ and $x_2 = v_a + 0.618 * (v_b - v_a)$, respectively. Then calculate the corresponding peak amplitudes of the average matched-filtering results of N subpulses of $\bar{\Re}_{peak}(x_1)$ with $v_{ref} = x_1$ and $\bar{\Re}_{peak}(x_2)$ with $v_{ref} = x_2$, respectively. Next, we turn to Step 3).

Step 3): Compare $\bar{\Re}_{peak}(x_1)$ with $\bar{\Re}_{peak}(x_2)$, if $\bar{\Re}_{peak}(x_1) = \bar{\Re}_{peak}(x_2)$, it means that the accurate velocity has been achieved. In practical signal processing with noise existing in the echo, we compare $|\frac{\bar{\Re}_{peak}(x_1)}{\bar{\Re}_{peak}(x_2)} - 1|$ and set a very small threshold ε, e.g., 0.0001. If $|\frac{\bar{\Re}_{peak}(x_1)}{\bar{\Re}_{peak}(x_2)} - 1| < \varepsilon$, we go to Step 5), otherwise we go to Step 4).

Step 4): If $\bar{\Re}_{peak}(x_2) > \bar{\Re}_{peak}(x_1)$, we set $v_a = v_a$ and $v_b = x_2$; otherwise if $\bar{\Re}_{peak}(x_2) < \bar{\Re}_{peak}(x_1)$, we set $v_a = x_1$ and $v_b = v_b$. Then we go back to Step 2).

Step 5): We get an accurate estimation of velocity as $x = \frac{x_1 + x_2}{2}$ and stop searching.

3.2. Coherent Bandwidth Synthesis

After the accurate velocity estimation is obtained, it is used for motion compensation, i.e., it is used for matched-filtering on the echo signal to get the spectrum of each subpulse. Then we coherently synthesize the spectra of all subpulses of the whole burst to get a much wider signal spectrum, on which inverse fast Fourier transform (IFFT) is performed and finally high-resolution range imaging is obtained [17, 42–44].

The formulation of coherently synthesized wide-band spectrum is

$$S_{syn}(f) \approx \sum_{n=1}^{N}\sum_{k=1}^{K} \tilde{A}_k \left|S(t_n, f - c_n\Delta f)\right|^2 \cdot \exp\left\{\frac{-j4\pi[f - c_n\Delta f]\Delta R_k}{c}\right\} \tag{23}$$

The synthesized bandwidth is $(N-1)\Delta f + B \approx N\Delta f$, hence the corresponding range resolution is about N times higher than that of a single subpulse signal. Thus high-resolution range imaging is obtained by:

$$s(t) = IFFT\{S_{syn}(f)\} \tag{24}$$

4. SIMULATION

4.1. Frequency-Hopping Code

In the simulation, the length of frequency-hopping code is 20, the quantization length is 16 bit, the difference of the initial values of these two CCM sequences is just the smallest quantization cell, i.e., $\frac{1}{2^{15}}$, and $m = 3$ is used. Figure 3 shows the CCM sequence and the corresponding frequency-hopping codes.

Even though the initial values are just tinily different, the generated two CCM sequences are very different. In addition, the frequency-hopping code corresponding to the first CCM sequence is [0, 15, 12, 16, 14, 10, 6, 13, 2, 8, 9, 7, 11, 1, 5, 17, 19, 18, 3, 4], while the frequency-hopping code corresponding to the second CCM sequence is [0, 16, 1, 5, 18, 7, 4, 15, 6, 13, 9, 11, 17, 10, 3, 2, 19, 8, 14, 12]. Only the first elements of the two frequency-hopping codes are the same, while the others are completely different. Therefore, we can control the frequency-hopping code by simply changing the initial value of a CCM sequence.

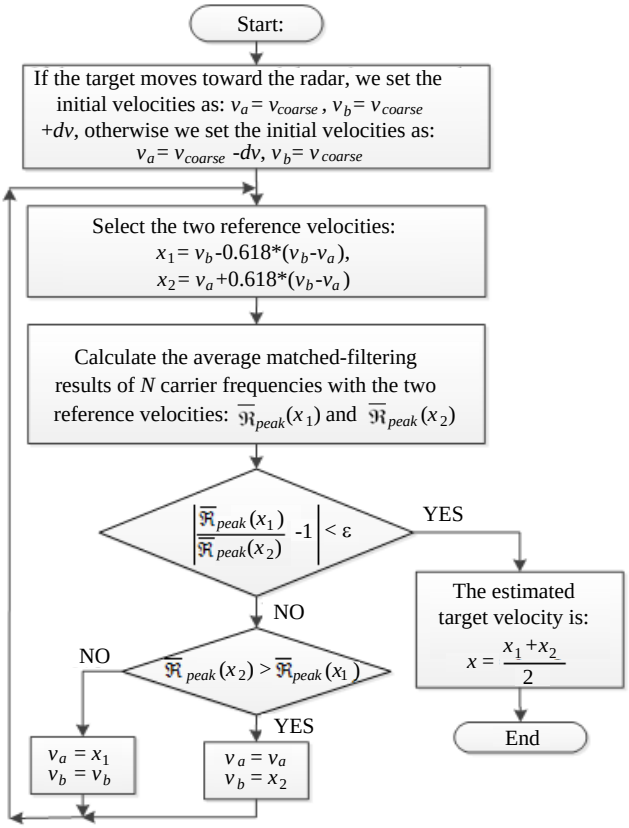

Figure 2. Algorithm diagram for accurate velocity estimation by GSS algorithm.

4.2. Ambiguity Function of CCM-FM Signal

In the simulation, the TD and the bandwidth of the generated CCM-FM signal are respectively 10 µs and 100 MHz, the carrier frequency is 34 GHz and the quantization length is 16 bit. Meanwhile, a Chirp signal with the same parameters is also simulated for comparison.

Figure 4 shows that the ambiguity function of the CCM-FM signal is thumbtack, and the peak locates where both the velocity and the range are zero. However, the ambiguity function of the Chirp signal is ridge-like, even if the velocity deviation is larger than the velocity resolution there still appears a peak after matched filtering. In fact, the peak appears at $f_d = k\tau$, where f_d is the Doppler frequency, k is the chirp rate and τ is the delay time [32].

Next, we plot both the range cut and the velocity cut of the ambiguity function. As shown in Figure 5, both the range resolutions of CCM-FM signal and Chirp signal are 1.5 m, which just corresponds to the 100 MHz bandwidth. However, the sidelobes of CCM-FM signal and Chirp signal are −22.86 dB and −13.45 dB, respectively. Meanwhile, both the velocity cuts of CCM-FM signal and Chirp signal are the same SINC function. This is because the time-domain amplitudes of both CCM-FM

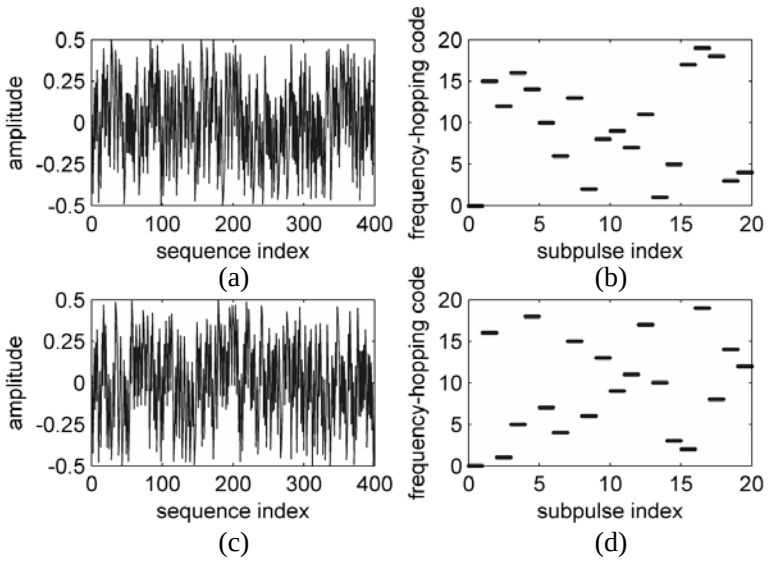

Figure 3. Comparison of CCM sequences and their corresponding frequency-hopping codes, whose initial values are different with just a quantization cell. (a) The first CCM sequence with a random initial value. (b) Frequency-hopping code corresponding to the first CCM sequence. (c) The second CCM sequence with an initial value just a quantization cell larger than that of the first one. (d) Frequency-hopping code corresponding to the second CCM sequence.

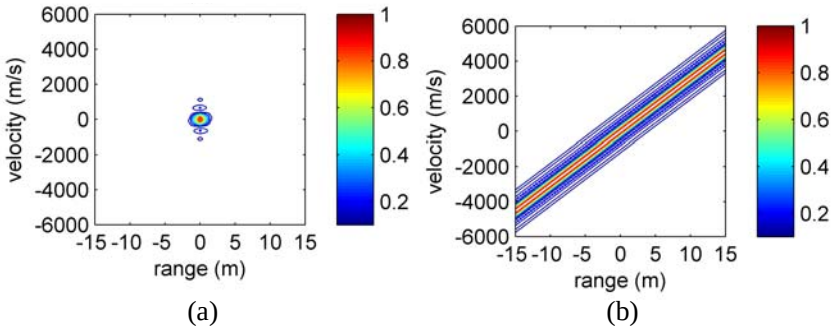

Figure 4. Normalized ambiguity function of (a) CCM-FM signal, as well as that of (b) chirp signal.

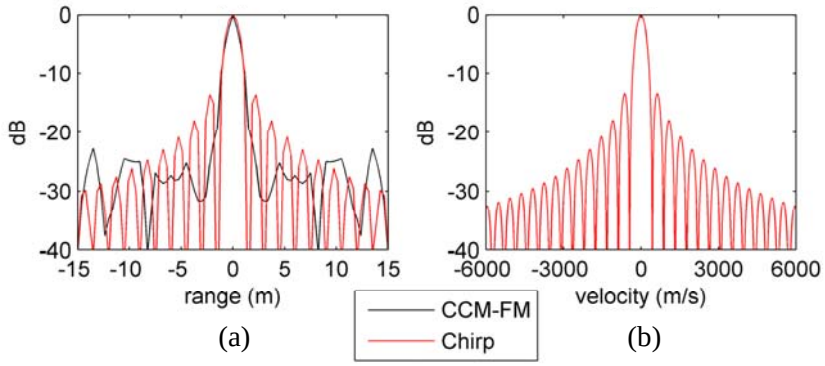

Figure 5. (a) Range cut and (b) velocity cut of the ambiguity function of CCM-FM signal, as well as those of Chirp signal.

Table 2. Normalized matched filtering outputs at different velocities.

Velocity		0 m/s	220 m/s	440 m/s	660 m/s	880 m/s
CCM-FM signal	Peak	0 dB	−3.88 dB	no peak	no peak	no peak
	Location	0 m	0 m	no peak	no peak	no peak
Chirp signal	Peak	0 dB	0 dB	0 dB	0 dB	0 dB
	Location	0 m	0.75 m	1.5 m	2.25 m	3 m

signal and Chirp signal are the same rectangle window. The velocity resolution is about 441 m/s, which is just accordance with Eq. (13).

In addition, we compare the peak amplitudes and their corresponding locations obtained from the matched filtering outputs at different velocities, as shown in Table 2. For the Chirp signal, the peaks still appear even though the velocity is larger than the velocity resolution, and the peak locations are different when the velocities are different. This is because the ambiguity function of a Chirp signal is ridge-like, where the range and the velocity couples with each other. Therefore, the range and velocity of moving targets cannot be distinguished by just one single Chirp signal.

However, for CCM-FM signal, the peaks appear only when the velocity is less than the velocity resolution, and all the peaks locate at range position of 0 m. When the velocity is larger than the velocity resolution, there will be no peaks any more. This is due to the thumbtack ambiguity function of CCM-FMs, where the range and the velocity are decoupled. Therefore, we can simultaneously estimate the range and the velocity of a moving target by using just one single CCM-FM signal.

4.3. High-Resolution Imaging of Moving Targets

Table 3 lists the simulation parameters of high-resolution one-dimensional imaging for high-speed moving targets. The subpulse bandwidth is 105 MHz, and the corresponding range resolution is about 1.5 m, so with single subpulse we cannot distinguish the four targets in Table 3. However, the synthesized bandwidth can be as large as 2005 MHz, and thus the corresponding range resolution can be as high as 0.075 m, so the four targets can be totally distinguished after bandwidth synthesis. The highest carrier frequency is 34 GHz, and the TD is 10 μs, so the velocity resolution is about 441 m/s according to Eq. (13). The frequency step is smaller than the subpulse bandwidth in order to suppress the grating lobes.

The subpulse interval is 15 μs and the number of subpulse is 20, so the burst time is 300 μs. The acceleration is 200 m/s^2, so the velocity variation in a burst is 0.06 m/s^2, which is just deviate 0.00067% relative to the targets' velocity and can be ignored in signal processing.

Table 3. Parameters for high-resolution range imaging of high-speed moving targets.

Subpulse TD (T_p)	10 μs
Subpulse interval (T_r)	15 μs
Subpulse bandwidth (B)	105 MHz
First carrier frequency (f_0)	32.1 GHz
Stepped frequency (Δf)	100 MHz
Number of stepped frequency (N)	20
Synthesized bandwidth	2005 MHz
Targets initial location	[49998, 49998.5, 50002, 50003] m
Normalized targets RCS	[1, 1, 1, 1]
Velocity	9000 m/s
Acceleration	200 m/s^2
SNR of echo signal	10 dB

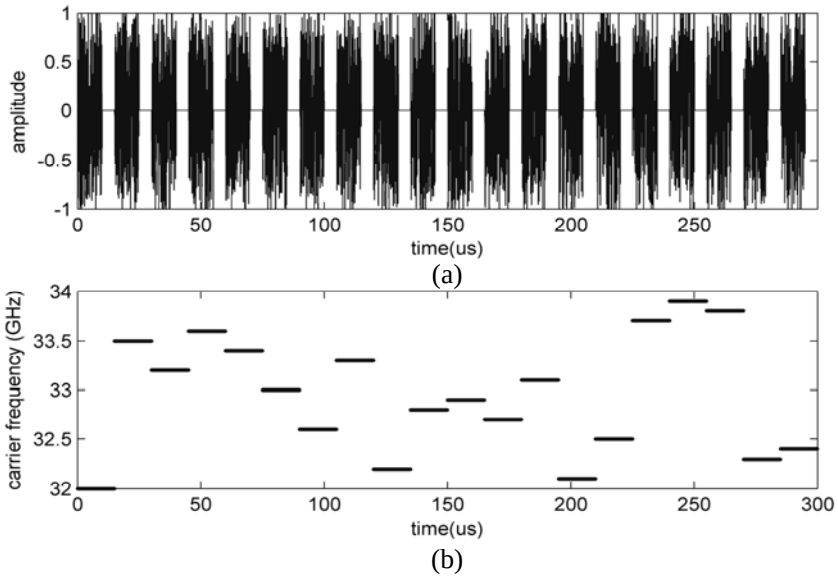

Figure 6. Transmitted randomly stepped noise signal waveforms, the upper (a) is the inphase components of the baseband signals and the lower (b) is the randomly stepped carrier frequencies.

Figure 6 shows the transmitted randomly stepped noise signal waveforms, where the upper is the inphase components of the baseband CCM-FM signals and the lower is the randomly stepped carrier frequencies. As one can see, the baseband CCM-FM signals have random waveforms, and they are different with each other. At the same time, the stepped carrier frequencies also exhibit the random property.

Figure 7 shows the average subpulse matched-filtering results of 20 subpulses at different reference velocities. We can see that when the deviation between the reference velocity and targets' velocity is larger than the velocity resolution, there is no prominent peak. However, when the deviation is less than the velocity resolution, e.g., when the reference velocity is 8690 m/s and the deviation is just 310 m/s, the average matched-filtering result exhibits two prominent peaks.

The threshold of peak-average ratio in coarse search is set as 20 dB and the step of coarse search set as $\frac{dv}{4} \approx 110$ m/s. Figure 8 shows the reference velocity and the peak-average ratio of matched-filtering output in each step, from which one can see that when the velocity deviations are larger than the

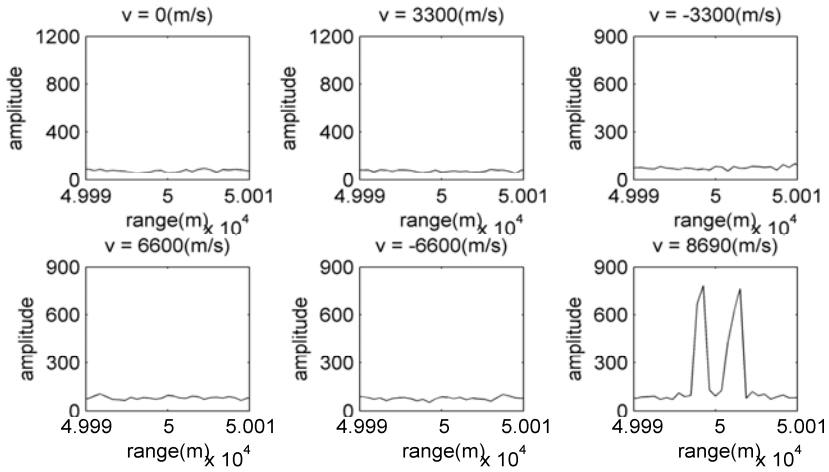

Figure 7. Average subpulse matched-filtering results of 20 subpulses at different reference velocities.

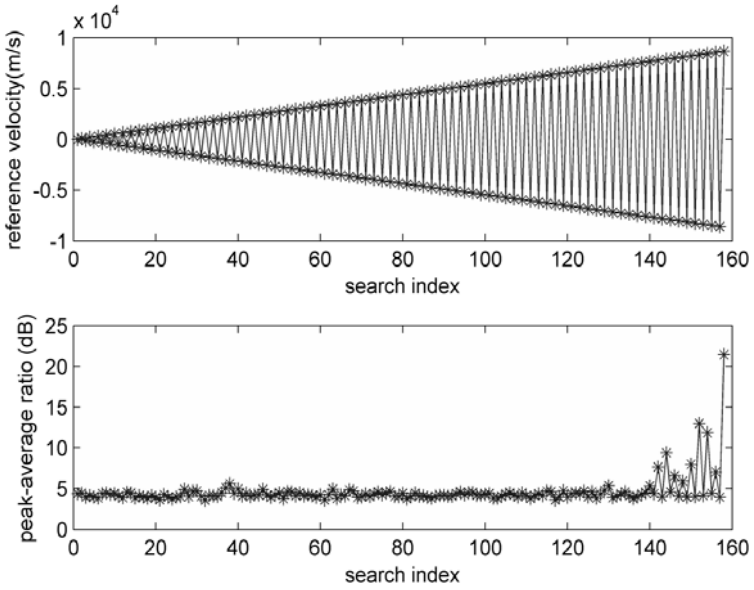

Figure 8. Peak-average ratios of matched-filtering results along with coarse search steps, the upper is the reference velocity in each step, while the lower the peak-average ratio of matched-filtering results.

velocity resolution, the peak-average ratios are much smaller than 20 dB. However, when the deviations are less than the velocity resolution, the peak-average ratios are close to or larger than 20 dB. The coarse search is terminated when the reference velocity reaches to 8690 m/s with the peak-average ratio being as large as 21.58 dB.

Table 4 shows the precise velocity search steps and the corresponding results. There are nine steps in total in the precise search procedure. One can see that, as the search step goes on, the velocity estimation is more and more close to the targets' true velocity, and finally we get the precise velocity estimation as $(8995.83 + 9005.19)/2 = 9000.52$ m/s with a relative error of just 0.0058%. It is to say we can accurately estimate the targets' velocity by using just a burst of subpulses.

After obtaining the precise velocity estimation, the velocity induced phase of a moving target can be accurately compensated and then it can be treated as a stationary target. With that we can conduct coherent bandwidth synthesis and show the synthesized spectrum in Figure 9, whose bandwidth is about 2 GHz.

Table 4. Precise velocity search steps and the corresponding results.

Search index	1	2	3	4	5
a (m/s)	8690	8858.08	8961.95	8961.95	8961.95
b (m/s)	9130	9130	9130	9065.80	9053.113
$\frac{\Re_{peak}(x_1)}{\Re_{peak}(x_2)}$	0.10704	0.94056	1.3169	1.0466	0.98617
Search index	6	7	8	9	
a (m/s)	8986.47	8986.47	8995.83	8995.83	
b (m/s)	9026.13	9010.98	9010.98	9005.19	
$\frac{\Re_{peak}(x_1)}{\Re_{peak}(x_2)}$	1.0074	0.99846	1.0014	0.99996	

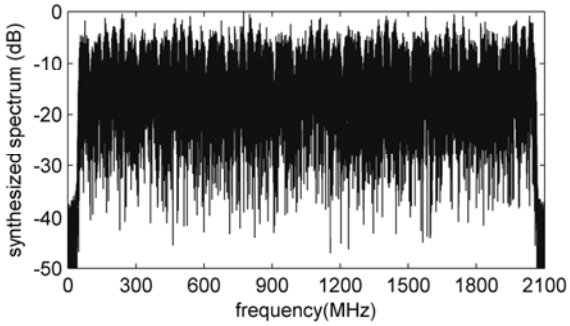

Figure 9. Synthesized power spectrum.

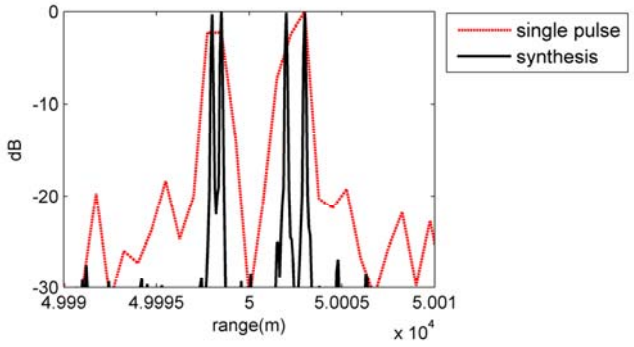

Figure 10. Final high-resolution range imaging result of four high-speed moving targets as compared with that of just a single subpulse.

Figure 10 shows the final high-resolution range imaging result as compared with that of just a single subpulse. The distance between the 1st and the 2nd targets is 0.5 m, and that between the 3th and the 4th targets is 1 m, i.e., they are smaller than the range resolution of a single subpulse. Therefore, the 1st and 2nd targets cannot be distinguished using just a single subpulse, and the same is true for the 3th and 4th targets. However, after coherent bandwidth synthesis, the range resolution reaches to 0.075 m, so all the four targets are clearly differentiated.

5. CONCLUSION

This paper proposes a burst model of chaotic noise signals with their carrier frequencies stepped randomly for velocity estimation and high-resolution range imaging of high-speed moving targets. The random stepping of carrier frequencies is controlled by a CCM sequence. The simulations show that even though the initial values are tinily different, the resulted frequency-hopping codes are completely different. Therefore, we can simply change the initial value to control the frequency-hopping code.

The baseband noise signal adopts the CCM-FM signal, which has a thumbtack ambiguity function. Therefore, the range and the velocity are independent with each other, and it is good for estimating the range and the velocity of a moving target simultaneously.

Based on the investigated signal with thumbtack ambiguity function, we propose a search algorithm to estimate the target velocity by using just a burst of subpulses. The search algorithm includes a coarse search and a precise search. The coarse search is conducted with a fixed step, which can make the velocity deviation less than the velocity resolution. The precise search adopts the GSS algorithm, which can lead to very accurate velocity estimation. After the accurate velocity is obtained, the velocity induced

phases can be compensated for all the subpulses, then their echoes can be coherently synthesized and finally high-resolution range imaging is achieved. Simulation results validate the effectiveness of the signal model and the processing algorithm.

REFERENCES

1. Li, N.-J. and Y.-T. Zhang, "A survey of radar ECM and ECCM," *IEEE Transactions on Aerospace and Electronic Systems*, Vol. 31, 1110–1120, 1995.
2. Spezio, A. E., "Electronic warfare systems," *IEEE Transactions on Microwave Theory and Techniques*, Vol. 50, 633–644, 2002.
3. Maksimov, M. V., M. Bobnev, L. N. Shustov, B. Krivitskii, G. I. Gorgonov, V. Ilin, et al., *Radar Anti-jamming Techniques*, Artech House, Inc., Dedham, Massachusetts, 1979.
4. Schleher, D. C., "Low probability of intercept radar," *International Radar Conference*, 346–349, 1985.
5. Lukin, K. and K. Kulpa, "Noise radar technology," *International Radar Symposium*, Wroclaw, Poland, 2008.
6. Garmatyuk, D. S. and R. M. Narayanan, "ECCM capabilities of an ultrawideband bandlimited random noise imaging radar," *IEEE Transactions on Aerospace and Electronic Systems*, Vol. 38, 1243–1255, 2002.
7. Liu, G., H. Gu, and W. Su, "Development of random signal radars," *IEEE Transactions on Aerospace and Electronic Systems*, Vol. 35, 770–777, 1999.
8. Zhang, Q., T.-S. Yeo, and G. Du, "ISAR imaging in strong ground clutter using a new stepped-frequency signal format," *IEEE Transactions on Geoscience and Remote Sensing*, Vol. 41, 948–952, 2003.
9. Wen, L., L. Teng, and Y. Han, "Moving targets imaging for stepped frequency radar," *5th International Conference on Signal Processing Proceedings*, Vol. 3, 1851–1855, Beijing, China, 2000.
10. Axelsson, S. R. J., "Analysis of ultra wide band noise radar with randomized stepped frequency," *International Radar Symposium*, 1–4, Krakow, Poland, 2006.
11. Liu, Z., B. Deng, and X. Wei, "Modified stepped-frequency train of LFM pulses," *International Conference on Information and Automation (ICIA)*, 1137–1141, Zhangjiajie, China, 2008.
12. Levanon, N., "Stepped-frequency pulse-train radar signal," *IEE Proceedings — Radar, Sonar and Navigation*, Vol. 149, 297–309, 2002.
13. Wehner, D. R., *High Resolution Radar*, Artech House, Norwood, MA, 1987.
14. Dang, H., "Stepped frequency chirp signal SAR imaging," *1st Asian and Pacific Conference on Synthetic Aperture Radar*, 14–18, Huangshan, China, 2007.
15. Yu, T., L. Chi, Y.-Q. Feng, C.-D. Li, and F. Zhu, "A coherent jamming approach of frequency-stepped chirp ISAR," *Modern Radar*, Vol. 7, 013, 2010.
16. Li, Y. and H.-L. Chen, "Study on deception jamming against stepped-frequency ISAR," *Xiandai Leida (Modern Radar)*, Vol. 29, 80–84, 2007.
17. Gu, X., Y. Zhang, and X. Zhang, "Stepped frequency random noise uwb radar signal," *3rd International Asia-Pacific Conference on Synthetic Aperture Radar (APSAR)*, 1–4, Seoul, 2011.
18. Hamilton, A. R. and R. D. Tollefson, "Frequency searching and/or jamming means," United States Patent, 1981.
19. Gonzalez-Blanco, P., E. de Diego, E. Millan, B. Errasti, and I. Montiel, "Stepped-frequency waveform radar demonstrator and its jamming," *International Waveform Diversity and Design Conference*, 192–196, Kissimmee, FL, 2009.
20. Narayanan, R. M., J. O. Curtis, Y. Xu, and P. D. Hoffmeyer, "Design, performance, and applications of a coherent ultra-wideband random noise radar," *Optical Engineering*, Vol. 37, 1855–1869, 1998.
21. Narayanan, R. M. and M. Dawood, "Doppler estimation using a coherent ultrawide-band random noise radar," *IEEE Transactions on Antennas and Propagation*, Vol. 48, 868–878, 2000.

22. Narayanan, R. M. and X. Xu, "Principles and applications of coherent random noise radar technology," *Proceedings of SPIE*, 503–514, 2003.
23. Lukin, K. A., "Radar design using noise/random waveforms," *International Radar Symposium*, 1–4, Krakow, Poland, 2006.
24. Ashtari, A., G. Thomas, H. Garces, and B. C. Flores, "Radar signal design using chaotic signals," *International Waveform Diversity and Design Conference*, 353–357, Pisa, Italy, 2007.
25. Yang, Q., Y. Zhang, and B. Li, "FPGA-based real-time generator of combination chaotic frequency-modulated signal for noise radar," *PIERS Proceedings*, 534–536, Guangzhou, China, Aug. 25–28, 2014.
26. Chua, M. Y. and V. C. Koo, "FPGA-based chirp generator for high resolution UAV SAR," *Progress In Electromagnetics Research*, Vol. 99, 71–88, 2009.
27. Yang, Q., Y. Zhang, and X. Gu, "A signal model based on combination chaotic map for noise radar," *Progress In Electromagnetics Research M*, Vol. 28, 57–71, 2013.
28. Zhang, Y., J. Wu, and H. Li, "Two simple and efficient approaches for compressing stepped chirp signals," *Asia-Pacific Conference Proceedings Microwave Conference Proceedings*, 4, Suzhou, China, 2005.
29. Levanon, N. and E. Mozeson, "Nullifying ACF grating lobes in stepped-frequency train of LFM pulses," *IEEE Transactions on Aerospace and Electronic Systems*, Vol. 39, 694–703, 2003.
30. Schuster, H. G., *Deterministic Chaos: An Introduction*, Fourth, Revised and Enlarged Edition, WILEY-VCH Verlag, Weinheim, 2005.
31. Flores, B. C., E. A. Solis, and G. Thomas, "Assessment of chaos-based FM signals for range-Doppler imaging," *IEE Proceedings — Radar, Sonar and Navigation*, Vol. 150, 313–322, 2003.
32. Levanon, N. and E. Mozeson, *Radar Signals*, Wiley & Sons, Inc., New Jersey, 2004.
33. Bassem, R. and Z. Atef, *Matlab Simulations for Radar Systems Design*, CRC Press, USA, 2004.
34. Richards, M. A., *Fundamentals of Radar Signal Processing*, Tata McGraw-Hill Education, New York, USA, 2005.
35. Ashtari, A., G. Thomas, W. Kinsner, and B. C. Flores, "Sufficient condition for chaotic maps to yield chaotic behavior after FM," *IEEE Transactions on Aerospace and Electronic Systems*, Vol. 44, 1240–1248, 2008.
36. Oppenheim, A. V., A. S. Willsky, and S. H. Nawab, *Signals and Systems*, Prentice Hall, New Jersey, 1997.
37. Luenberger, D. G., *Introduction to Linear and Nonlinear Programming*, Addison-Wesley Reading, MA, 1973.
38. Yuan, Y. and W. Sun, *Optimization Theory and Methods*, Science Press, Beijing, China, 1997.
39. Luenberger, D. G. and Y. Ye, *Linear and Nonlinear Programming*, Springer Science & Business Media, New York, USA, 2008.
40. Riming, S. and C. Liuchen, "A new maximum power point tracking method for photovoltaic arrays using golden section search algorithm," *Canadian Conference on Electrical and Computer Engineering*, 619–622, Ontario, Canada, 2008.
41. Agrawal, J. and M. Aware, "Golden section search (GSS) algorithm for maximum power point tracking in photovoltaic system," *5th International Conference on Power Electronics (IICPE)*, 1–6, Delhi, 2012.
42. Zhai, W. and Y. Zhang, "A stepped frequency chirp scaling algorithm for high resolution SAR imaging," *3rd International Asia-Pacific Conference on Synthetic Aperture Radar (APSAR)*, 1–4, Seoul, Korea, 2011,
43. Zhao, L., J. Mu, X. J. Fu, and M. Gao, "A novel method of ISAR imaging for high speed targets using stepped-frequency chirp waveform," *IEEE CIE International Conference on Radar (Radar)*, 1604–1607, Chengdu, China, 2011.
44. Yuan, H., M. Gao, and G. Liu, "Coherent spectrum synthesis of frequency-stepped chirp signal," *IET International Radar Conference*, 1–4, Guilin, China, 2009.